FACULDADE DE ENGENHARIA DA UNIVERSIDADE DO PORTO

Design of an Asynchronous Flash Analog-to-Digital Converter

Gonçalo Pinto Monteiro

STATE OF ART

Mestrado em Engenharia Eletrotécnica e de Computadores

Supervisor: Prof. Manuel Cândido Duarte dos Santos

Second Supervisor: João Pedro Santos

January 9, 2026

Abstract

The proliferation of Internet of Things and biomedical sensors has created a high demand for low-power signal processing interfaces. In many of these applications, the signals of interest are sparse, characterized by long periods of inactivity. Classical synchronous Analog-to-Digital Converters are inherently inefficient in such scenarios, as they consume dynamic power continuously due to the global clock, regardless of the input signal activity.

This dissertation proposes the design and implementation of an Asynchronous Flash ADC. By removing the clock, the proposed architecture aligns power consumption with the input signal activity, theoretically achieving a much lower power consuption. However, the removal of the clock introduces design challenges (acrescentar aqui problemas)

To address this, an offline trimming strategy is proposed to calibrate the comparator offsets without compromising the high-speed operation of the flash topology. The work encompasses the theoretical analysis, schematic design, and validation of the system through Analog/Mixed-Signal co-simulation. The expected outcome is a robust, clockless ADC architecture that offers a superior Figure of Merit for sparse signal applications in compared to conventional synchronous architectures.

Keywords: Analog-to-Digital Converter, Asynchronous Design, Flash ADC, Level-Crossing Sampling, Offset Trimming, Low Power, IoT.

Contents

List of Figures

List of Tables

List of Acronyms

Chapter 1

Introduction

This chapter provides a brief introduction to the topic associated with the work carried out during the dissertation period. Firstly, a contextualization is given, followed by a presentation of the research question and the main motivations for carrying out this study. The main objectives of this dissertation will also be outlined, as well as the methodology used to achieve them. Finally, the structure of the dissertation is presented.

We live in an era where smart devices are everywhere, known as the Internet of Things, IoT. While the processing and storage of information are inherently digital, benefiting from the scaling of Moore's Law, the physical world remains fundamentally analogic. Physical variables such as temperature, sound and biological potentials are continuous in both time and amplitude. Consequently, the Analog-to-Digital Converter, ADC, serves as the critical interface bridging these two domains, enabling digital systems to interact with the real world [**johns_martin_2012**].

Energy efficiency has shifted from being a secondary performance metric to a primary design constraint, many of the sensors operate on limited battery or rely on energy harvesting, where every Joule of power dissipation has a direct effect on the system's autonomy. In this landscape, the data conversion block almost always takes place as the most spender in this field, especially in sensor interfaces where the digital transmission is duty-cycled.

However, a fundamental characteristic of many environmental and physiological signals is sparsity in between pulses. Signals such as electrocardiograms, voice activity, or environmental monitoring data are spread in bursts in nature: they contain short periods of high information content followed by long intervals of inactivity.

Traditional data conversion approaches, based on uniform sampling and dictated by the Nyquist-Shannon theorem [**shannon_1949**], treat these silence periods with the same computational power and energetic waste as the active periods. This creates a paradigm of inefficiency the system dissipates power to generate redundant digital samples that carry no new information. Recognizing and exploiting this sparsity is the key to unlocking ultra-low-power electronic interfaces.

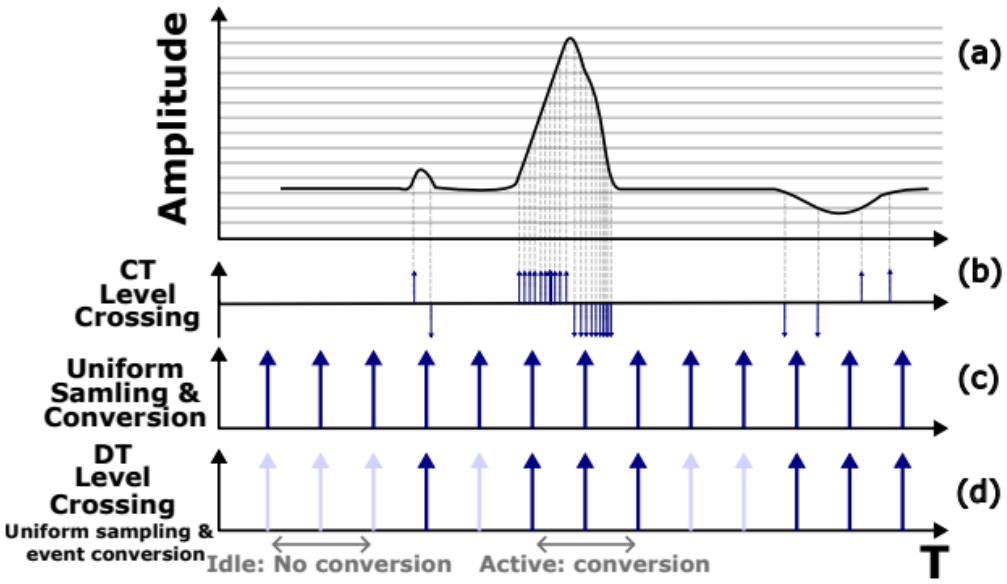

Figure 1.1: Time-sparse signal representation and sampling strategies. (a) Time-sparse signal example showing burst activity with periods of inactivity. (b) Continuous-time event-driven sampling and conversion, which responds to signal changes. (c) Conventional uniform sampling operating at fixed Nyquist rate regardless of signal activity. (d) Discrete-time sampling with event-driven conversion, combining periodic and event-based approaches. This illustration demonstrates the efficiency of adaptive sampling methods for sparse signals compared to uniform sampling at the Nyquist rate [**lim_2013**].

1.1 Motivation and Problem Statement

The energy waste in massive-scale IoT deployments and the inefficiency of conventional synchronous architectures when processing sparse data shows the need for a fundamental shift toward architectures that activate only when meaningful data events occur.

1.1.1 Inefficiency of Synchronous Sampling

Traditional Analog-to-Digital Converters operate under a fixed-rate sampling rate, dictated by a global clock signal (f_s). As established by the Nyquist-Shannon sampling theorem [**shannon_1949**], this rate is determined by the maximum possible bandwidth of the signal, $f_s \geq 2B$. However, in many real-world applications, the signal is often active for only a fraction of the time, meaning the true information content is much lower than the theoretical maximum bandwidth suggests.

This leads to a massive waste of energy due to the fundamental relationship governing dynamic power consumption in CMOS circuits [**baker_cmos_2010**]:

$$P_{dynamic} = \alpha \cdot f \cdot C_L \cdot V_{DD}^2 \tag{1.1}$$

where:

- $P_{dynamic}$ is the dynamic power dissipated.
- α is the activity factor (or switching factor).
- f is the clock frequency.
- C_L is the load capacitance being switched (e.g., in the clock tree).

1.1.2 Architectural Problem: Flash ADCs

While the Flash ADC architecture is highly attractive due to its single-cycle, high-speed conversion capability [**johns_martin_2012**], it suffers from severe limitations regarding power and area, particularly when reaching medium-to-high resolution. The number of required comparators scales exponentially with resolution (2^N). This exponential scaling leads directly to an increase in input capacitance and static power dissipation.

Even in low-power, synchronous designs, the dynamic power of the comparator switching is the dominant factor in the power budget.

Therefore, combining the high speed of the Flash architecture with the high power efficiency required for IoT demands a radical shift away from the synchronous clocking scheme.

1.1.3 Device Limitation: The Mismatch Problem

To mitigate the power and area issues mentioned above, designers are compelled to minimize the physical dimensions of the core devices, particularly the transistors within the comparators. However, this introduces a fundamental physical constraint:

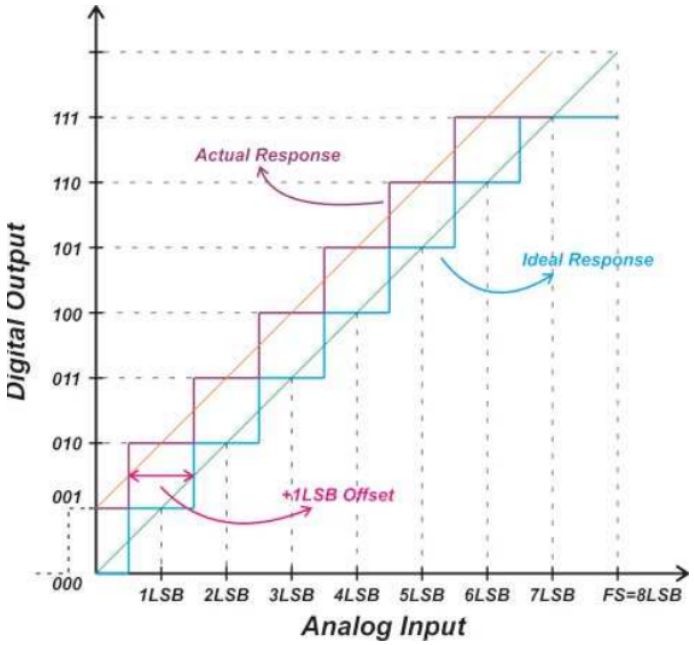

Figure 1.2: Input offset voltage (V_{os}) generation in CMOS comparators due to transistor mismatch. The figure illustrates how random variations in threshold voltage (V_{th}) and gain factor (β) in the differential input pair result in an offset voltage that shifts the trip point of the comparator [**johns_martin_2012**]. This mismatch-induced offset becomes the primary limitation for converter accuracy in deep-submicron technologies.

The reduction of transistor size, while increasing speed and reducing capacitance, drastically increases random variations in parameters like the threshold voltage (V_{th}), leading to a significant Input Offset Voltage (V_{os}) in the comparators [**baker_cmos_2010**].

1.2 Objectives and Contribution

Based on the limitations identified in traditional synchronous data conversion when dealing with sparse sensor signals, the primary objective of this work is to design and implement an energy-efficient ADC architecture, so this ADC must exploit signal inactivity to achieve a significant reduction in power consumption.

1.2.1 Specific Objectives

To achieve the overall goal of developing an efficient ADC, the following specific objectives are defined for this dissertation:

1. Asynchronous Architecture Design: To develop the circuit-level design of an asynchronous Flash ADC, minimizing dynamic power consumption by ensuring that power is only dissipated when an input signal event occurs.

2. Offline Trimming Implementation: To implement an offline trimming mechanism capable of detecting and compensating for the input offset voltage of the comparators.

3. Mixed-Signal Validation: To validate the complete system through analog and digital co-simulation. This validation must confirm the functionality and accuracy of both the asynchronous core and the trimming logic.

4. Performance Benchmarking: To quantify the energy efficiency of the proposed design using well known figures of merit. The results must be compared against the current state of the art synchronous ADCs and relevant asynchronous solutions.

Chapter 2

Literature Review

This chapter presents the state-of-the-art in Analog-to-Digital Converters, reviewing theoretical foundations and analyzing survey data to justify the proposed architecture.

2.1 Fundamentals of Analog-to-Digital Conversion

This section provides the theoretical background required to understand the operation and performance characterization of data converters. It covers the fundamental steps of the conversion process such as sampling, quantization, and coding.

2.1.1 The Data Conversion Process

2.1.1.1 Ideal Data Conversion

The analog-to-digital conversion process acts as the bridge between the continuous physical world and the discrete digital domain. Conceptually, it involves two distinct operations: discretization in time, sampling, and discretization in amplitude, quantization. Ideally, this process should be instantaneous and lossless within the signal bandwidth of interest [**johns_martin_2012**].

2.1.1.2 The Sampling Operation

Sampling converts a continuous-time signal $x(t)$ into a discrete-time sequence $x[n]$ [**johns_martin_2012**].

According to the Nyquist-Shannon sampling theorem [**shannon_1949**], a band-limited signal with maximum frequency B can be perfectly reconstructed if the sampling frequency f_s satisfies:

$$f_s \geq 2B \tag{2.1}$$

Violating this condition results in aliasing, where high-frequency spectral components mixes into the baseband, becoming indistinguishable from the original signal [**johns_martin_2012**].

2.1.1.3 The Quantization Operation

While sampling transforms continuous time in discrete values, quantization maps the continuous amplitude of each sample to one of a finite number of levels [**johns_martin_2012**]. An N-bit ADC divides the input range (V_{ref}) into 2^N discrete levels. The step size between adjacent levels is the Least Significant Bit (LSB):

$$V_{LSB} = \frac{V_{ref}}{2^N} \tag{2.2}$$

Unlike sampling, quantization is non-reversible and introduces a deterministic error. This error is typically modeled as white noise added, the quantization noise with a uniform probability distribution. For an ideal quantizer, the Signal-to-Quantization-Noise Ratio (SQNR) is given by the formula [**johns_martin_2012**]:

$$SQNR_{dB} \approx 6.02N + 1.76 \tag{2.3}$$

2.1.1.4 Coding

The final stage is encoding the quantized level into a binary format. The choice of coding scheme being the most common straight binary and gray code which depends on the system requirements for data processing and transmission, but does not affect the fundamental analog performance [**baker_cmos_2010**].

2.1.2 Performance Metrics

To evaluate and compare different data converters objectively, a standard set of metrics is used [**johns_martin_2012**]. These are categorized into dynamic and static parameters.

2.1.2.1 Resolution and Sampling Rate

Resolution defines the theoretical dynamic range, while the sampling rate determines the maximum signal bandwidth. However, these are nominal values the actual performance is limited by noise and non-linearities [**johns_martin_2012**].

2.1.2.2 Signal-to-Noise-Distortion Ratio (SNDR)

Signal to noise ratio adding distortion ratio or SNDR is the primary dynamic metric [**johns_martin_2012**]. It is the ratio of the signal power to the total power of all noise and harmonic distortion components. From SNDR, the Effective Number of Bits, ENOB, is derived [**johns_martin_2012**]:

$$ENOB = \frac{SNDR_{dB} - 1.76}{6.02} \tag{2.4}$$

This value represents the true resolution of the converter at a specific input frequency.

2.1.2.3 Differential and Integral Non-Linearity (DNL and INL)

Static linearity is characterized by measuring the deviation of code transition levels from their ideal positions [**johns_martin_2012**]. The DNL measures the deviation of a single step width from the ideal 1 LSB. A DNL less than -1 LSB implies a missing code in the transfer function.

The INL is the cumulative sum of DNL errors, representing the deviation of the transfer curve from a straight line. Specific INL patterns like saw-tooth shapes can reveal systematic errors in the architecture, such as gain mismatch or non-linear biasing [**van_de_plassche_1994**].

2.1.2.4 Offset and Gain Error

These are linear errors, offset is a constant shift of the transfer characteristic as seen before in section 1.2.3, while gain error is a deviation in the slope [**johns_martin_2012**]. Unlike non-linearity, these errors preserve the signal shape and can often be calibrated out simply.

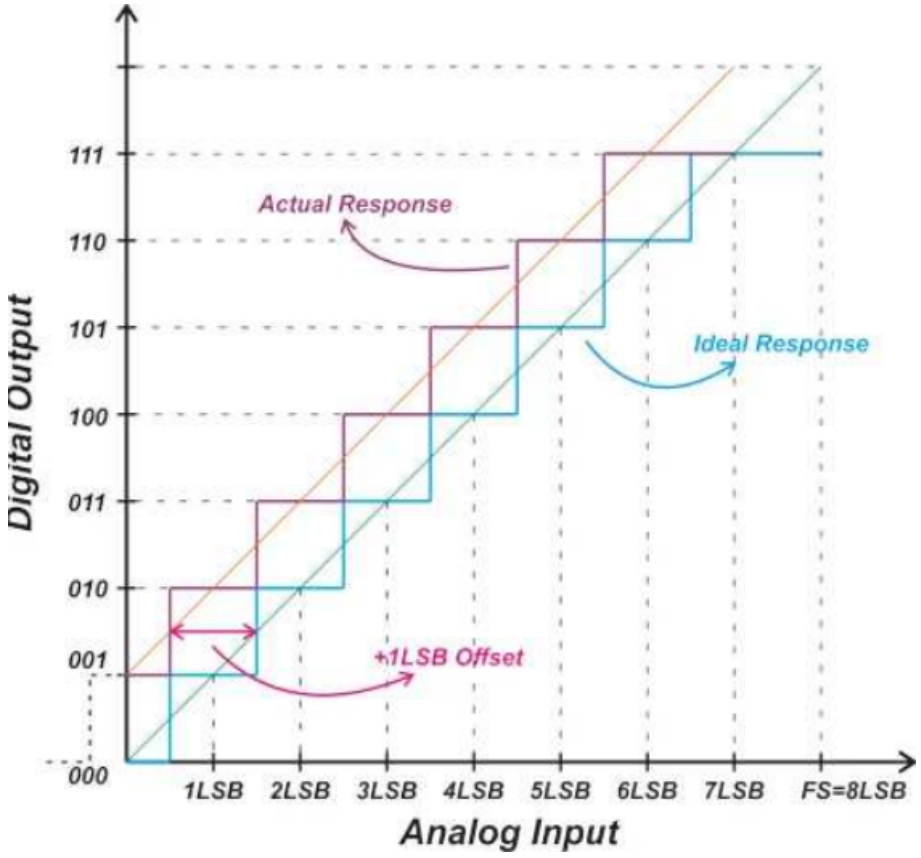

Figure 2.1: ADC transfer function showing offset and gain errors. Offset error represents a constant DC shift applied uniformly across all codes, while gain error modifies the slope of the transfer function. Both are linear errors that can be calibrated using digital post-processing techniques [**johns_martin_2012**].

2.1.2.5 Bit Error Rate (BER)

BER quantifies the probability of the converter producing an incorrect digital code [**baker_cmos_2010**]. This is often caused by metastability, a phenomenon where internal decision circuits fail to resolve a valid logic level within the allocated time when the input is extremely close to a decision threshold.

2.1.3 State-of-the-Art Comparative Analysis

The analytical plots and tables presented below incorporate data from an exhaustive set of 140 state-of-the-art works. To ensure transparency and reproducibility, the complete list of references used to generate these performance envelopes—covering Flash, SAR, Pipeline, and Sigma-Delta architectures—is provided in [1–138]. Collectively, these works represent the proven performance frontier across all major ADC architectures.

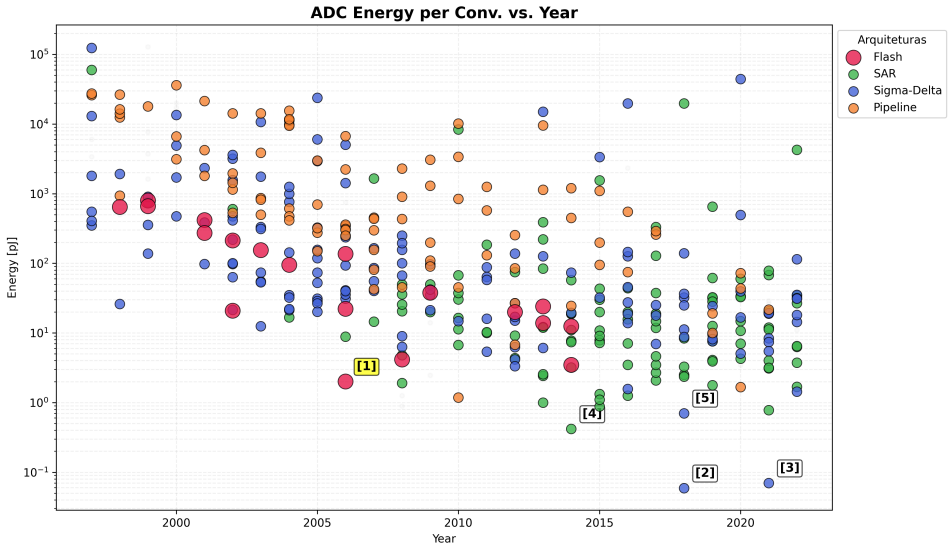

Figure 2.2: Energy per conversion step vs. Year of publication (ISSCC dataset).

Table 2.1: Energy per Conversion vs. Year (Flash reference [1] highlighted)

Ref.	Architecture	Publication	Energy [pJ]
[1]	**Flash**	**Chen [Chen_2006]**	**2.02**
[2]	Sigma-Delta	Jiang [**Jiang_2018**]	0.059
[3]	Sigma-Delta	Veldhoven [**Veldhoven_2021**]	0.070
[4]	SAR	Ginsburg [**Ginsburg_2014**]	0.420
[5]	Sigma-Delta	Kim [**Kim_2018**]	0.703

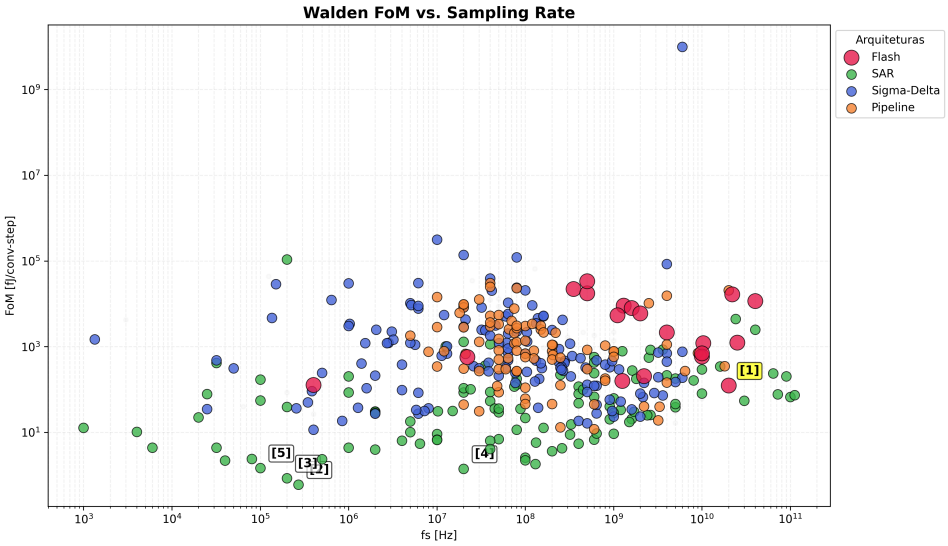

Figure 2.3: Walden FoM vs. Sampling Rate (f_s).

Table 2.2: Walden FoM vs. Sampling Frequency (Flash reference [1] highlighted)

Ref.	Architecture	Publication	f_s [Hz]
[1]	**Flash**	**Lukas [Lukas_2014]**	**20G**
[2]	SAR	Jang [**Jang_2018**]	270k
[3]	SAR	Ginsburg [**Ginsburg_2014**]	200k
[4]	SAR	Cano [**De_Cano_Garcia_2019**]	20M
[5]	SAR	Muller [**Muller_2015**]	200

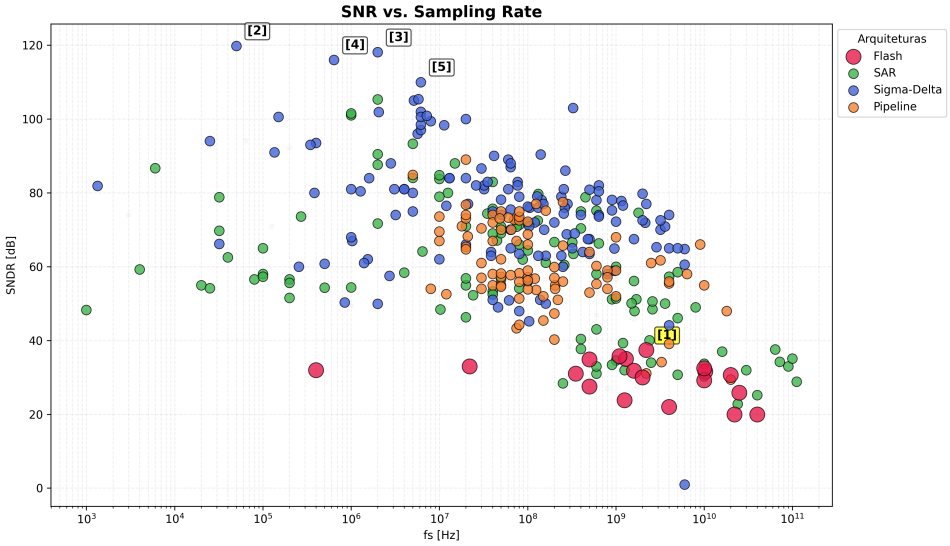

Figure 2.4: SNDR vs. Sampling Frequency (f_s) comparison.

Table 2.3: SNDR vs. Sampling Frequency (Flash reference [1] highlighted)

Ref.	Architecture	Publication	SNDR [dB]
[1]	**Flash**	**Draxelmayr [Draxelmayr_2014]**	**37.4**
[2]	Sigma-Delta	Delic [**Delic-Ibus_2013**]	120.0
[3]	Sigma-Delta	Jang [**Jang_2018_2**]	118.0
[4]	Sigma-Delta	Abe [**Abe_2016**]	116.0
[5]	Sigma-Delta	Geelen [**Geelen_1997**]	110.0

2.2 Synchronous Architectures

To address asynchronous ADCs we first need to address synchronous ADCs, they have a global clock signal that dictates sampling instances and synchronizes internal operations. While these architectures are highly mature and widely used, they face fundamental power efficiency trade-offs, particularly when operating at high frequencies or processing sparse data [**johns_martin_2012**].

2.2.1 Synchronous Flash ADC

The Flash ADC is conceptually the simplest and fastest architecture, performing a complete conversion in a single clock cycle [**baker_cmos_2010**]. It utilizes a resistive ladder to generate $2^N - 1$ reference voltages, which are compared simultaneously to the input signal by a large bank of comparators. This parallel comparison produces a thermometer code, that a digital logic block then

converts into a standard binary output. Its primary limitation is the exponential increase in hardware complexity, area, and power consumption as resolution increases.

The thermometer term refers to the parallel output from the Flash ADC comparators, where '1's run up to the input voltage level like mercury in a thermometer, indicating signal strength before being converted to standard binary by an encoder.

2.2.2 The Power Bottleneck

The primary drawback of the synchronous Flash architecture is its exponential scaling. Survey data clearly illustrates that high speed translates into high power in these designs. For example, a 6-bit 500 MS/s CMOS Flash ADC reported in 1999 already consumed 400 mW [**Tamba**].

More extreme cases, such as a 22 GS/s 5-bit design, can consume up to 1.2 W [**Schvan_2006**].

The continuous clocking of a massive comparator bank creates a significant energy dissipation even when the input signal is static. This lack of adaptivity makes synchronous Flash architectures increasingly unsuitable for battery-powered or energy-harvesting applications.

2.2.3 SAR (Successive Approximation Register)

The SAR ADC operates using a binary search algorithm [**van_de_plassche_1994**], for each sample the internal logic tests one bit at a time, starting from the most significant bit (MSB). A single comparator compares the input to the output of an internal digital to analog converter (DAC), if the input is higher, the bit is set to '1' otherwise, it is set to '0'. This process repeats for N cycles. Because it uses very few active components, it is the most energy efficient choice for low speeds.

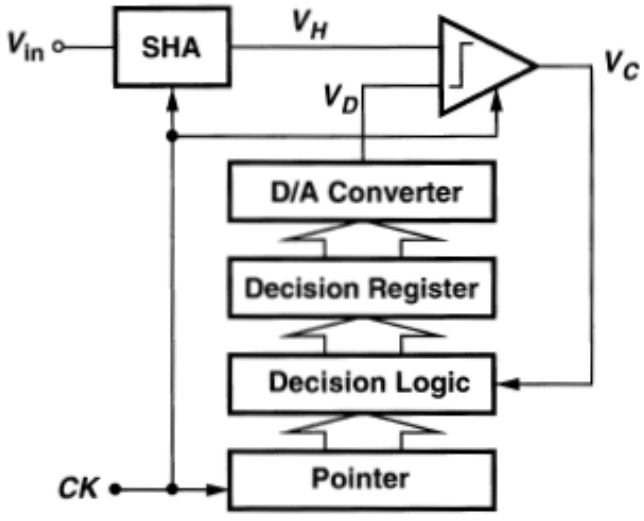

Figure 2.5: Successive Approximation Register (SAR) ADC architecture showing the binary search algorithm implementation. The architecture consists of a DAC, a single comparator, and binary search logic that successively tests each bit from MSB to LSB, resulting in N clock cycles for an N-bit conversion. The main advantage is energy efficiency due to the use of a single comparator and minimal active circuitry [**van_de_plassche_1994**].

2.2.4 Pipeline

The Pipeline ADC breaks the conversion into several sequential stages [**johns_martin_2012**], each stage resolves a few bits of information, quantizes them, and passes the remaining error, the residue, to the next stage after amplification. This approach allows the ADC to work on multiple samples concurrently, obtaining very high throughput and high resolution, the problem relies in the inherent processing latency.

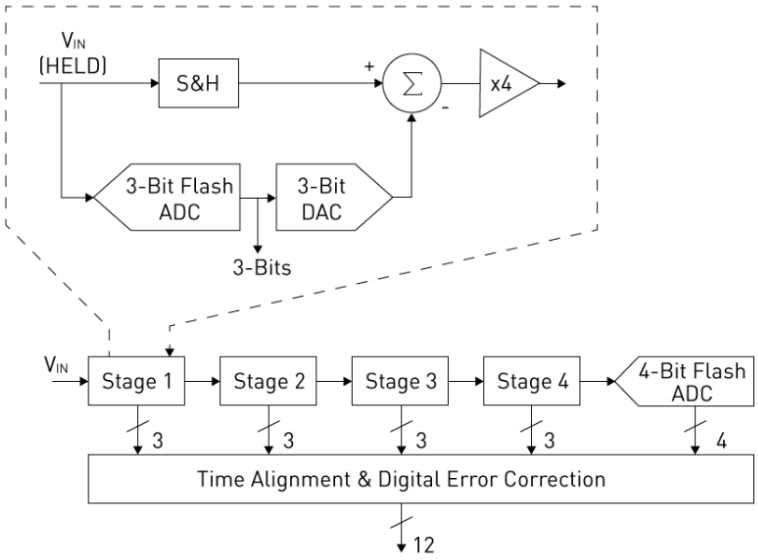

Figure 2.6: Pipeline ADC architecture showing multiple conversion stages operating in parallel on different input samples. Each stage resolves a portion of the bits and amplifies the residual error to the next stage. The pipelined structure enables high-throughput operation at the expense of increased latency and circuit complexity [**johns_martin_2012**].

2.2.5 Sigma-Delta (ΣΔ)

The ΣΔ architecture relies on oversampling, sampling much faster than the Nyquist rate [**candy_1985**], and noise-modulation. A modulator integrates the difference between the input signal and a feedback version of the quantized output. This process pushes the quantization noise into higher frequencies, outside the signal band of interest, a digital filter then removes the high-frequency noise, resulting in high resolution and precision [**schreier_2005**].

2.2.6 Dual-slope

This integrating architecture [**microelectronics_1998**] measures the time required for a capacitor to charge and discharge, in the first phase, the capacitor is charged by the input voltage for a fixed period then for the second phase, it is discharged by a known reference voltage. The time it takes to return to zero is proportional to the average value of the input signal it's highly accurate and immune to high-frequency noise but is much slower than other architectures.

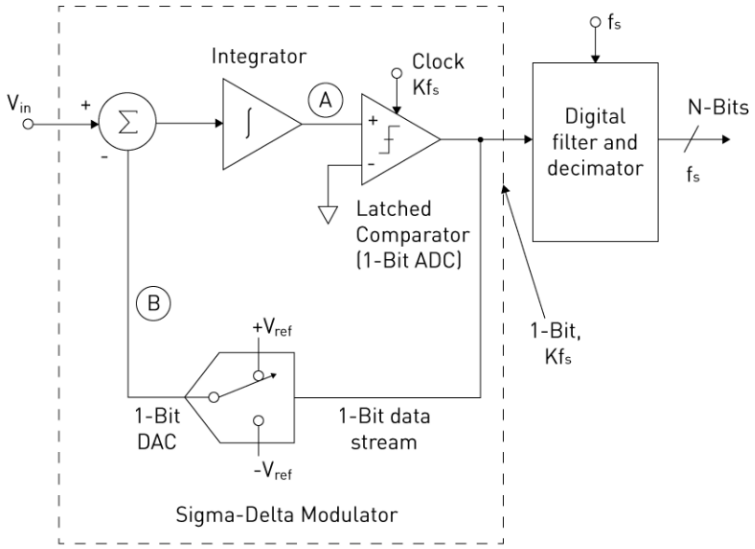

Figure 2.7: First-order Sigma-Delta modulator architecture showing the integrator, quantizer, and feedback path. The modulator operates at a clock frequency much higher than the Nyquist rate, and the quantization noise is shaped to frequencies outside the signal band, allowing digital filtering to recover high-resolution signals [**candy_1985**].

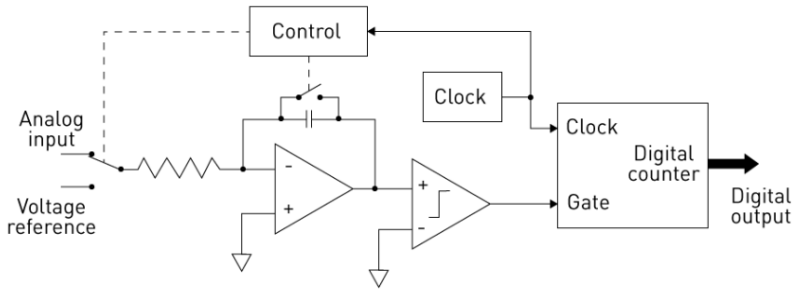

Figure 2.8: Dual-slope (integrating) ADC architecture showing the charging phase where an unknown input signal is integrated for a fixed time, and the discharge phase where a precise reference voltage drives the capacitor back to zero. The conversion time is proportional to the input voltage, providing excellent accuracy and noise rejection at the expense of low throughput [**microelectronics_1998**].

2.3 Asynchronous Architectures

Asynchronous, or event-driven, architectures represent a fundamental paradigm shift in data conversion [**lim_2013**], unlike synchronous ADCs, which are bound by a global clock and the Nyquist-Shannon sampling theorem, asynchronous ADCs operate based on the signal's activity. This approach offers a more efficient alternative for processing sparse signals.

2.3.1 Level-Crossing Sampling (LCS)

The core principle behind many asynchronous ADCs is Level-Crossing Sampling (LCS) [**lim_2013**]. In traditional uniform sampling, the signal is captured at fixed time intervals (T_s), and the amplitude is quantized. In LCS, the process is inverted: the amplitude levels are fixed (quantization thresholds), and the ADC records the exact time at which the input signal crosses these thresholds.

This method is particularly powerful for signals that remain constant or change slowly over long periods. Instead of generating redundant samples that capture no new information, the LCS ADC remains idle, only producing a digital event when the signal effectively changes by more than the defined threshold.

2.3.2 Asynchronous Flash ADC

The Asynchronous Flash ADC adapts the parallel structure of a standard Flash ADC but removes the sampling clock entirely. In this architecture, the comparators are not latched by a clock, they operate in continuous time, constantly monitoring the input voltage V_{in} against the reference ladder. The event generation happens when the input signal crosses a threshold, the corresponding comparator changes its output state immediately, this transition triggers an asynchronous logic to generate a digital output pulse.

2.4 Calibration and Trimming Techniques

In high-speed Flash ADCs, the accuracy of the system is fundamentally limited by the precision of the comparators. While the architecture fundamentals were established in the previous sections, practical implementations must address the non-idealities of the fabrication process, specifically the Input Offset Voltage (V_{os}).

2.4.1 The Component Mismatch Problem

In deep sub-micron CMOS technologies, transistors that are drawn with identical dimensions on the layout will exhibit slight differences in their electrical parameters after fabrication. This phenomenon, known as mismatch, affects the threshold voltage (V_{th}) and the current gain factor (β) of the differential pair in a comparator [**baker_cmos_2010**].

According to Pelgrom's Law cited in section 2.3.3 of [**johns_martin_2012**], the standard deviation of the threshold voltage mismatch (σ_{Vth}) is inversely proportional to the square root of the transistor area ($W \cdot L$):

$$\sigma_{V_{th}} = \frac{A_{V_{th}}}{\sqrt{W \cdot L}} \tag{2.5}$$

Where $A_{V_{th}}$ is a technology-dependent constant. This creates a critical trade-off, to minimize offset without calibration, transistors must be made large, which increases parasitic capacitance and degrades the ADC speed and power efficiency. Therefore, small transistors are used for speed, and calibration is needed to correct the resulting offset.

2.4.2 Calibration Classifications

Calibration techniques can be broadly categorized by their timing and domain [**baker_cmos_2010**]. In terms of timing there can be derived two types foreground calibration which interrupts normal operation to measure and correct errors and background calibration which operates continuously but adds significant complexity. In terms of domain there is digital calibration that corrects the output code mathematically, whereas analog calibration adjusts the circuit biasing or load conditions to nullify the offset at the source.

For an asynchronous architecture, avoiding continuous clock activity is crucial to maintain low power during idle periods. Thus, Analog Foreground Calibration is the preferred approach.

2.4.3 Resistive Trimming Techniques

Resistive trimming aims to compensate for the imbalance in the input differential pair (M_1, M_2) by intentionally creating an opposing imbalance in the load resistance or the reference path [**baker_cmos_2010**].

2.4.3.1 Internal Resistive Loading

The internal resistive loading method involves placing a variable resistive network in parallel or series with the output loads of the comparator pre-amplifier stage. By digitally switching small resistors or MOS switches operating in the triode region in parallel with the load branch, the effective resistance R_L is modulated. Since the gain of the pre-amplifier is defined as $A_v = g_m R_L$, changing R_L on one side of the differential pair adjusts the output DC level. If the differential pair has an offset, the trimming network is adjusted to introduce an equal and opposite value to effectively zero the error. This technique is typically implemented using a binary-weighted bank of PMOS transistors as the variable resistance, where the digital control code is determined at startup and stored in a register.

2.4.3.2 Resistive Reference Ladder Trimming

The resistive reference ladder trimming technique corrects comparator offset by utilizing the main reference ladder as a calibration source [**yao_bulk_2011**]. In this architecture, a switching network

selects specific voltage taps from the resistor ladder and applies them to the bulk terminals of the input transistors M1 and M2. This approach leverages the body effect to shift the threshold voltage (V_{th}) of the differential pair, thereby nullifying the input-referred offset caused by process mismatch.

As demonstrated in the simulation results of the threshold voltage ($|V_t|$) versus the ladder tap voltage (LT), the threshold voltage of transistors M1 and M2 increases linearly from approximately 356.5 mV to 372 mV as the calibration voltage is adjusted. In contrast, the threshold voltage of transistors M3 and M4 remains constant at approximately 356.5 mV because their bulk terminals are not connected to the tuning network. This targeted adjustment of the bulk potential for the input differential pair provides a tuning range sufficient to compensate for random process variations and ensure the accuracy of the comparator trip points.

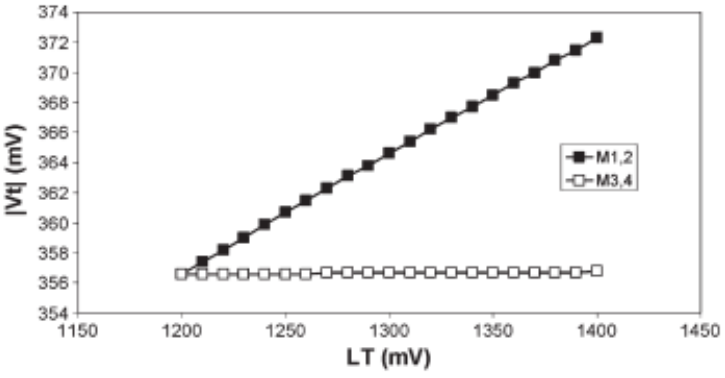

Figure 2.9: Threshold voltage ($|V_t|$) variation of input differential pair transistors (M1, M2) and load transistors (M3, M4) as a function of the resistive ladder tap voltage (LT). The graph demonstrates the body effect: as the bulk potential of M1 and M2 is modulated via the reference ladder, their threshold voltage increases linearly, providing a calibration range to compensate for process-induced mismatch. In contrast, M3 and M4 maintain constant V_{th} since their bulk terminals are connected to fixed substrate potential. This selective tuning is the basis of the proposed resistive ladder trimming mechanism [**yao_bulk_2011**].

2.4.4 Advantages of Resistive Trimming for Asynchronous ADCs

Compared to dynamic techniques like Auto-Zeroing which requires accurate clock phases ϕ_1, ϕ_2 and storage capacitors [**baker_cmos_2010**], resistive trimming offers distinct advantages for the proposed work:

1. Static Operation: Once the calibration bits are set (during the offline phase), the trimming network becomes static. It does not switch and does not require a clock, preserving the "event-driven" nature of the ADC.

2. Speed Preservation: It does not add significant capacitive load to the high-speed nodes of the comparator, allowing for maximum bandwidth.

2.5 Related Works

As high-speed and low-power Analog-to-Digital Converters become increasingly critical for modern integrated systems, the Flash architecture remains a preferred choice due to its parallel operation and low latency. However, at high resolutions and speeds, transistor mismatch in the comparator array poses a significant challenge, leading to increased offset voltages. To address these limitations, various research efforts have focused on current-mode techniques and optimized comparator structures.

The research proposed in this dissertation differs from the established literature by focusing on an asynchronous level-crossing sampling Flash ADC, which deviates from the synchronous current-mode architectures. While most current-mode designs rely on specialized conveyors or algorithmic cycles, the approach developed here utilizes a bulk-driven offset trimming mechanism. By modulating the threshold voltage (V_{th}) via the body effect through a resistive reference ladder [**yao_bulk_2011**], this work achieves precise offset nullification without the high power overhead of complex biasing or the speed penalties of synchronous clocking.

2.6 Asynchronous vs. Synchronous

2.6.1 Advantage

The primary motivation for adopting asynchronous architectures is the direct relationship between signal activity and power consumption [**lim_2013**].

In a synchronous system, the clock tree and the comparators switch at every clock cycle, regardless of whether the input is changing, the power consumption is dominated by the fixed clock frequency [**baker_cmos_2010**]:

$$P_{sync} \approx f_{clk} \cdot C_{total} \cdot V_{DD}^2 \tag{2.6}$$

In an asynchronous ADC, the switching frequency is replaced by the event rate. If the signal is constant or slowly varying, the comparators and digital logic remain static, leading to the following proportionality:

$$P_{async} \propto Activity \times V_{DD}^2 \tag{2.7}$$

This property ensures that the energy consumed is always proportional to the information content of the signal which makes these ADCs significantly more efficient for sparse signal environments, where they can achieve near-zero power during periods of inactivity.

2.6.2 Comparative Evaluation

An analysis of state-of-the-art converters shows that asynchronous ADCs excel in energy efficiency across a wide range of sampling rates, particularly for low-to-medium bandwidths [**lim_2013**].

While Synchronous Flash ADCs are designed for peak performance at a specific frequency and suffer from a much higher power consumption caused by the continuous clocking, asynchronous designs scale their power consumption linearly with the input activity.

Table 2.4: Comparison of Power Consumption between Synchronous and Asynchronous Flash ADCs. Simulation results from this work showing the power advantage of asynchronous operation for sparse signals.

Topology	**Average power (P [W])**	**No of samples**
Synchronous	0.1016	145
Asynchronous	0.0314	23

The impact of this architectural difference on long-term technology trends is illustrated in Figure 2.10. The plot depicts the energy per conversion (P/f_s) over the last two decades. While both paradigms show a downward trend due to process node scaling, asynchronous designs (indicated by triangular markers) consistently occupy the lower bound of the energy envelope. This suggests that eliminating the global clock is a key enabler for breaking the power efficiency barriers in modern designs.

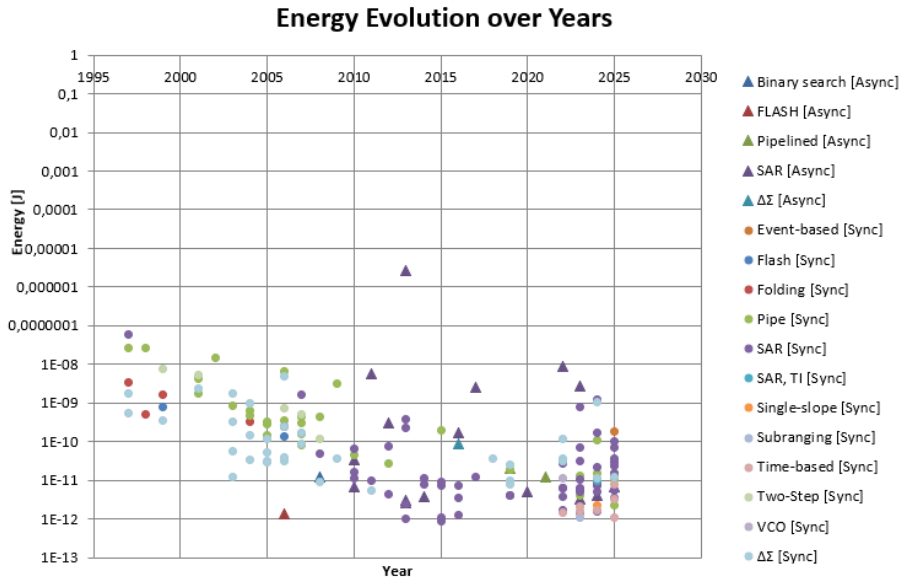

Figure 2.10: Energy per conversion evolution (P/f_s) over the years, highlighting the lower energy floor achieved by asynchronous designs. The triangular markers represent asynchronous ADC implementations, while circular markers represent synchronous designs. The plot demonstrates that asynchronous architectures consistently achieve lower energy consumption across multiple technology nodes compared to their synchronous counterparts, validating the energy efficiency advantage of event-driven operation. Data compiled from ISSCC publications (1997-2025) [**lim_2013**, **Tamba**, **Schvan_2006**, **Hammerschmied**, **Vorenkamp**, **Yong_In_Park**, **Ingino**, **Yoshioka_2010**, **Liu_2010**].

Chapter 3

Future Work Planning, Methodologies and Tools

This chapter outlines the development strategy for the dissertation, detailing the methodologies, tools, and the schedule for the remaining phases.

3.1 Work Plan

Since the work completed this far covers the introduction and the literature review, future planning focuses on the three remaining sections. Chapter 3 will detail the mathematical formulation of the asynchronous level-crossing sampling and the bulk voltage trimming mechanism. Chapter 4 will involve the implementation, simulation, and discussion of the results, while Chapter 5 will present the final conclusions and suggestions for future work. To complete the dissertation according to the established timeline and quality standards, a Gantt Chart is presented in Figure 3.1. The second semester will begin on February 18, 2026, with the development of the mathematical model for bulk-driven offset compensation, specifically focusing on the threshold voltage modulation via the body effect as discussed in the literature. This will be followed by the design and simulation of the asynchronous Flash ADC core and the resistive trimming network in the Cadence Virtuoso environment. Once the circuit achieves basic functionality, Monte Carlo simulations will be performed to evaluate the robustness of the trimming algorithm against random process mismatches. The results will then be analyzed to quantify improvements in linearity and energy efficiency. After the first version of the dissertation is finalized, a scientific research article will be prepared for submission. Regular meetings with the supervisors will be held throughout the process to ensure technical consistency. The provisional document will be delivered by June 30, 2026, with the defense scheduled for July 24, and the final document submission by July 31, 2026.

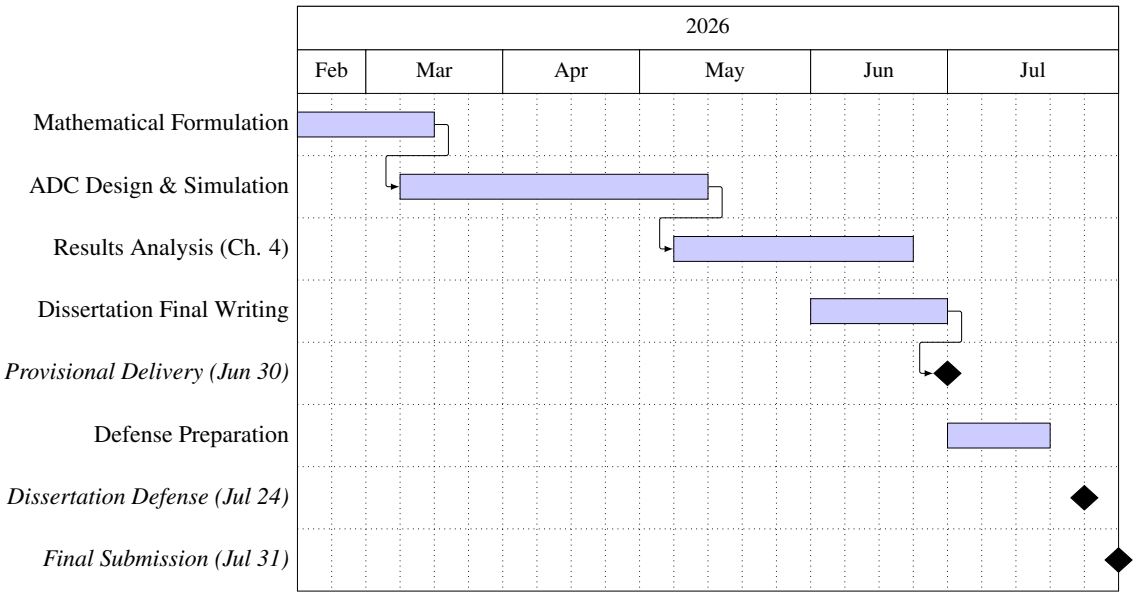

Figure 3.1: Dissertation work plan for the second semester of 2026.

3.2 Methodologies and Tools

The execution of this dissertation follows a methodology focused on academic rigor and effective project management to ensure all objectives are met. A primary practice involves the use of project management tools such as the Gantt chart presented in Figure 3.1 to establish clear milestones and monitor progress. By defining specific tasks and deadlines, it is possible to maintain a structured timeline and ensure that the research and design phases stay on schedule. Another fundamental practice consists of holding biweekly meetings with supervisors to review the work carried out and receive technical feedback. These sessions are essential for validating the circuit design choices and avoiding potential errors in the implementation of the asynchronous logic. Continuous documentation of the findings and simulation results is also prioritized to maintain transparency and facilitate the transition from the research phase to the final writing of the document.

For the development and verification of the proposed asynchronous Flash ADC, the Synopsys software will be used as the primary tool for circuit-level design and simulation. This professional toolset allows for precise transistor-level modeling and the verification of the offset trimming mechanism through analog and mixed-signal simulations.

Chapter 4

Conclusions

The work conducted during the first semester has been essential for establishing the technical and theoretical foundations of this dissertation. The increasing demand for high-speed, low-power ADCs in modern system on chip applications drives the need for innovative architectures that can overcome the limitations of traditional designs. In this context, the research into an asynchronous level-crossing sampling Flash ADC with bulk-driven offset trimming can significantly contribute to the development of more efficient data conversion systems for high-bandwidth applications.

A variety of ADC architectures and comparator topologies have been deeply studied to understand their performance trade-offs. The Flash architecture is recognized for its parallel processing capabilities, but its accuracy is often limited by transistor mismatch, which necessitates effective calibration or trimming techniques. Current-mode techniques have been explored as a means to achieve higher speeds and lower power consumption compared to traditional voltage-mode designs. Furthermore, the study of dynamic latch comparators and current conveyors has provided insights into optimizing the delay profile and power dissipation of the conversion core. This research has highlighted that asynchronous level-crossing sampling can reduce the power overhead associated with global clocks, especially during periods of signal inactivity. To address the mismatch inherent in these high-speed comparators, a bulk-driven trimming mechanism utilizing the body effect is proposed, allowing for precise threshold voltage modulation without adding significant parasitic capacitance.

An extensive investigation of existing studies in this field was conducted to ensure the acquisition of the knowledge necessary to develop the mathematical formulation of the proposed system. The bibliographic review confirmed that while current-mode and inverter-based comparators offer high performance, there is a clear opportunity to integrate them into an asynchronous framework with localized trimming. Once the mathematical model for the bulk potential adjustment is finalized, the main challenge ahead will be to prove the effectiveness and robustness of the proposed approach using Synopsys simulation tools. A rigorous analysis through Monte Carlo simulations will be pursued to validate the trimming algorithm against process variations, ensuring a successful trade-off between conversion speed, power efficiency, and linearity.

Bibliography

[1] Abhishek Agrawal et al. “A 128Gb/s 1.95pJ/b D-Band Receiver with Integrated PLL and ADC in 22nm FinFET”. In: *IEEE International Solid-State Circuits Conference (ISSCC)*. 2023. DOI: 10.1109/ISSCC42615.2023.10067439.

[2] B. Malki et al. “A 70dB DR 10b 0-80MS/s Current Integrating SAR ADC with adaptive Dynamic Range”. In: *IEEE International Solid-State Circuits Conference (ISSCC)*. 2012. DOI: 10.1109/ISSCC.2012.6177095.

[3] C-Y Liou et al. “A 2.4-to-5.2fJ/Conversion-step 10b 0.5-to-4MS/s SAR ADC with Charge Average Switching DAC in 90nm CMOS”. In: *IEEE International Solid-State Circuits Conference (ISSCC)*. 2013. DOI: 10.1109/ISSCC.2013.6487735.

[4] E. Janssen et al. “An 11b 3.6GS/s Time-Interleaved SAR ADC in 65nm CMOS”. In: *IEEE International Solid-State Circuits Conference (ISSCC)*. 2013. DOI: 10.1109/ISSCC.2013.6487816.

[5] P. Harpe et al. “A 2.2/2.7fJ/conversion-step 10/12b 40kS/s SAR ADC with Data-Driven Noise Reduction”. In: *IEEE International Solid-State Circuits Conference (ISSCC)*. 2013. DOI: 10.1109/ISSCC.2013.6487730.

[6] P. Harpe et al. “A 7-to-10b 0-to-4MS/s Flexible SAR ADC with 6.5-to-16fJ/conversion-step”. In: *IEEE International Solid-State Circuits Conference (ISSCC)*. 2012. DOI: 10.1109/ISSCC.2012.6177096.

[7] R. Kapusta et al. “A 14-bit, 80MS/s SAR ADC with 73.6dB SNDR in 65nm CMOS”. In: *IEEE International Solid-State Circuits Conference (ISSCC)*. 2013. DOI: 10.1109/ISSCC.2013.6487820.

[8] Y. Chai et al. “A 5.37mW 10b 200MS/s Dual-Path Pipelined ADC”. In: *IEEE International Solid-State Circuits Conference (ISSCC)*. 2012. DOI: 10.1109/ISSCC.2012.6177091.

[9] P. Balmelli and Qiuting Huang. “A 25 MS/s 14 b 200 mW ΣΔ modulator in 0.18 μm CMOS”. In: *IEEE International Solid-State Circuits Conference (ISSCC)*. 2004. DOI: 10.1109/ISSCC.2004.1332600.

[10] Rares Bodnar et al. “A 9.3nV/rtHz 20b 40MS/s 94.2dB DR Signal-Chain Friendly Precision SAR Converter”. In: *IEEE International Solid-State Circuits Conference (ISSCC)*. 2024. DOI: 10.1109/ISSCC49657.2024.10454329.

[11] H. H. Boo, D. S. Boning, and H-S. Lee. “A 12b 250MS/s Pipelined ADC with Virtual Ground Reference Buffers”. In: *IEEE International Solid-State Circuits Conference (ISSCC)*. 2015. DOI: 10.1109/ISSCC.2015.7063036.

[12] L.J. Breems et al. “A 56mW CT Quadrature Cascaded ΣΔ Modulator with 77dB DR in a Near Zero-IF 20MHz Band”. In: *IEEE International Solid-State Circuits Conference (ISSCC)*. 2007. DOI: 10.1109/ISSCC.2007.373382.

[13] K. Bult, A. Buchwald, and J. Laskowski. “A 170 mW 10 b 50 Msample/s CMOS ADC in 1 mm²”. In: *IEEE International Solid-State Circuits Conference (ISSCC)*. 1997. DOI: 10.1109/ISSCC.1997.585303.

[14] Yue Cao et al. “A 1GS/s Single-Channel Pipelined ADC with a Parallel-Operation SAR Sub-Quantizer and a Dynamic-Deadzone Ring Amplifier”. In: *IEEE International Solid-State Circuits Conference (ISSCC)*. 2025. DOI: 10.1109/ISSCC49661.2025.10904766.

[15] Yuefeng Cao et al. “A 12GS/s 12b 4× Time-Interleaved Pipelined ADC with Comprehensive Calibration of TI Errors and Linearized Input Buffer”. In: *IEEE International Solid-State Circuits Conference (ISSCC)*. 2024. DOI: 10.1109/ISSCC49657.2024.10454350.

[16] Yuefeng Cao et al. “A Single-Channel 12b 2GS/s PVT-Robust Pipelined ADC with Ringingless Ring Amplifier and Time-Domain Quantizer”. In: *IEEE International Solid-State Circuits Conference (ISSCC)*. 2023. DOI: 10.1109/ISSCC42615.2023.10067687.

[17] Y. Chae, I. Lee, and G. Han. “A 0.7V 36uW 85dB-DR Audio delta-sigma Modulator Using a Class-C Inverter”. In: *IEEE International Solid-State Circuits Conference (ISSCC)*. 2008. DOI: 10.1109/ISSCC.2008.4523271.

[18] C-H. Chan et al. “A 5.5mW 6b 5GS/s 4-times Interleaved 3b/cycle SAR ADC in 65nm CMOS”. In: *IEEE International Solid-State Circuits Conference (ISSCC)*. 2015. DOI: 10.1109/ISSCC.2015.7063128.

[19] Feng Chen, S. Ramaswamy, and B. Bakkaloglu. “A 1.5V 1mA 80dB passive ΣΔ ADC in 0.13μm digital CMOS process”. In: *IEEE International Solid-State Circuits Conference (ISSCC)*. 2003. DOI: 10.1109/ISSCC.2003.1234204.

[20] Zhuoyi Chen et al. “A 182.3dB FoMs 50MS/s Pipelined-SAR ADC using Cascode Capacitively Degenerated Dynamic Amplifier and MSB Pre-Conversion Technique”. In: *IEEE International Solid-State Circuits Conference (ISSCC)*. 2024. DOI: 10.1109/ISSCC49657.2024.10454297.

[21] Zhuoyi Chen et al. “An Easy-Drive 16MS/s Pipelined-SAR ADC Using Split Coarse-Fine Input Buffer Sampling Scheme and Fast-Robust Background Inter-Stage Gain Calibration”. In: *IEEE International Solid-State Circuits Conference (ISSCC)*. 2025. DOI: 10.1109/ISSCC49661.2025.10904526.

[22] Kai-Cheng Cheng et al. “A 94.3dB SNDR 184dB FoMs 4th-Order Noise-Shaping SAR ADC with Dynamic-Amplifier-Assisted Cascaded Integrator”. In: *IEEE International Solid-State Circuits Conference (ISSCC)*. 2024. DOI: 10.1109/ISSCC49657.2024.10454362.

[23] Kyojin D. Choo, John Bell, and Michael P Flynn. “Area-Efficient 1GS/s 6b SAR ADC with Charge-Injection-Cell-Based DAC”. In: *IEEE International Solid-State Circuits Conference (ISSCC)*. 2016. DOI: 10.1109/ISSCC.2016.7418106.

[24] T. Christen, T. Burger, and Qiuting Huang. “A 0.13μm CMOS EDGE/UMTS/WLAN Tri-Mode $\Delta\Sigma$ ADC with -92dB THD”. In: *IEEE International Solid-State Circuits Conference (ISSCC)*. 2007. DOI: 10.1109/ISSCC.2007.373383.

[25] A.L. Coban and P.E. Allen. “A 1.5 V 1.0 mW audio $\Delta\Sigma$ modulator with 98 dB dynamic range”. In: *IEEE International Solid-State Circuits Conference (ISSCC)*. 1999. DOI: 10.1109/ISSCC.1999.759091.

[26] Siddharth Devarajan et al. “A 16b 125MS/s 385mW 78.7dB SNR CMOS Pipeline ADC”. In: *IEEE International Solid-State Circuits Conference (ISSCC)*. 2009. DOI: 10.1109/ISSCC.2009.4977320.

[27] A. Dezzani and E. Andre. “A 1.2-V dual-mode WCDMA/GPRS $\Sigma\Delta$ modulator”. In: *IEEE International Solid-State Circuits Conference (ISSCC)*. 2003. DOI: 10.1109/ISSCC.2003.1234206.

[28] M. Ding et al. “A 5.5fJ/conv.step 6.4MS/s 13b SAR ADC utilizing a redundancy facilitated background error-detection and correction scheme”. In: *IEEE International Solid-State Circuits Conference (ISSCC)*. 2015. DOI: 10.1109/ISSCC.2015.7063125.

[29] L. Dorrer et al. “A 3mW 74dB SNR 2MHz CT $\Delta\Sigma$ ADC with a tracking-ADC-quantizer in 0.13 μm CMOS”. In: *IEEE International Solid-State Circuits Conference (ISSCC)*. 2005. DOI: 10.1109/ISSCC.2005.1494084.

[30] M. Flynn and B. Sheahan. “A 400Msample/s 6b CMOS folding and interpolating ADC”. In: *IEEE International Solid-State Circuits Conference (ISSCC)*. 1998. DOI: 10.1109/ISSCC.1998.672412.

[31] P. Fontaine, A.N. Mohieldin, and A. Bellaouar. “A low-noise low-voltage CT $\Delta\Sigma$ modulator with digital compensation of excess loop delay”. In: *IEEE International Solid-State Circuits Conference (ISSCC)*. 2005. DOI: 10.1109/ISSCC.2005.1494087.

[32] Y. Fujimoto et al. “An 80/100MS/s 76.3/70.1dB SNDR $\Delta\Sigma$ ADC for Digital TV Receivers”. In: *IEEE International Solid-State Circuits Conference (ISSCC)*. 2006. DOI: 10.1109/ISSCC.2006.1696049.

[33] R. Gaggl, M. Inversi, and A. Wiesbauer. "A power optimized 14-bit SC ΔΣ modulator for ADSL CO applications". In: *IEEE International Solid-State Circuits Conference (ISSCC)*. 2004. DOI: 10.1109/ISSCC.2004.1332604.

[34] Jihang Gao et al. "A 93.3dB SNDR, 180.4dB FoMS Calibration-Free Noise-Shaping Pipelined-SAR ADC with Cross-Stage Gain-Mismatch-Error-Shaping Technique and Negative-R-Assisted Residue Integrator". In: *IEEE International Solid-State Circuits Conference (ISSCC)*. 2025. DOI: 10.1109/ISSCC49661.2025.10904557.

[35] Govert Geelen and Edward Paulus. "An 8b 600MS/s 200mW CMOS folding A/D converter using an amplifier preset technique". In: *IEEE International Solid-State Circuits Conference (ISSCC)*. 2004. DOI: 10.1109/ISSCC.2004.1332690.

[36] Govert Geelen et al. "A 90nm CMOS 1.2V 10b Power and Speed Programmable Pipelined ADC with 0.5pJ/Conversion-Step". In: *IEEE International Solid-State Circuits Conference (ISSCC)*. 2006. DOI: 10.1109/ISSCC.2006.1696118.

[37] J. Goes et al. "A 0.9V Delta-Sigma Modulator with 80dB SNDR and 83dB DR Using a Single-Phase Technique". In: *IEEE International Solid-State Circuits Conference (ISSCC)*. 2006. DOI: 10.1109/ISSCC.2006.1696048.

[38] B. Gregoire and U-K. Moon. "An Over-60dB True Rail-to-Rail Performance Using Correlated Level Shifting and an Opamp with 30dB Loop Gain". In: *IEEE International Solid-State Circuits Conference (ISSCC)*. 2008. DOI: 10.1109/ISSCC.2008.4523296.

[39] Mingyang Gu et al. "A 12b 3GS/s Pipelined ADC with Gated-LMS-Based Piecewise-Linear Nonlinearity Calibration". In: *IEEE International Solid-State Circuits Conference (ISSCC)*. 2025. DOI: 10.1109/ISSCC49661.2025.10904536.

[40] C. Hammerschmied and Q. Huang. "A MOSFET-only, 10 b, 200 ksample/s A/D converter capable of 12 b untrimmed linearity". In: *IEEE International Solid-State Circuits Conference (ISSCC)*. 1997. DOI: 10.1109/ISSCC.1997.585301.

[41] Junyan Hao et al. "A Single-Channel 2.6GS/s 10b Dynamic Pipelined ADC with Time-Assisted Residue Generation Scheme Achieving Intrinsic PVT Robustness". In: *IEEE International Solid-State Circuits Conference (ISSCC)*. 2023. DOI: 10.1109/ISSCC42615.2023.10067822.

[42] P. Harpe, E. Cantatore, and A. van Roermund. "An Oversampled 12b/14b SAR ADC with Noise Reduction and Linearity Enhancements Achieving up to 79.1dB SNDR". In: *IEEE International Solid-State Circuits Conference (ISSCC)*. 2014. DOI: 10.1109/ISSCC.2014.6757396.

[43] P. Harpe et al. "A 3nW Signal-Acquisition IC Integrating an Amplifier with 2.1 NEF and a 1.5fJ/conv-step ADC". In: *IEEE International Solid-State Circuits Conference (ISSCC)*. 2015. DOI: 10.1109/ISSCC.2015.7063086.

[44] Xiyu He et al. “A 71dB SNDR 200MHz BW Interleaved Pipe-SAR ADC with a Shared Residue Integrating Amplifier Achieving 173dB FoMs”. In: *IEEE International Solid-State Circuits Conference (ISSCC)*. 2024. DOI: 10.1109/ISSCC49657.2024.10454431.

[45] Benjamin Hershberg et al. “A 3.2GS/s 10 ENOB 61mW Ringamp ADC in 16nm with Background Monitoring of Distortion”. In: *IEEE International Solid-State Circuits Conference (ISSCC)*. 2019. DOI: 10.1109/ISSCC.2019.8662290.

[46] M. Hesener et al. “A 14b 40MS/s Redundant SAR ADC with 480MHz Clock in 0.13pm CMOS”. In: *IEEE International Solid-State Circuits Conference (ISSCC)*. 2007. DOI: 10.1109/ISSCC.2007.373387.

[47] H-K. Hong et al. “A 2.6b/cycle-architecture-based 10b 1.7GS/s 15.4mW 4x Time-interleaved SAR ADC with a Multi-step Hardware Retirement Technique”. In: *IEEE International Solid-State Circuits Conference (ISSCC)*. 2015. DOI: 10.1109/ISSCC.2015.7063130.

[48] Gian Hoogzaad and Raf Roovers. “A 65 mW 10 b 40 Msample/s BiCMOS Nyquist ADC in 0.8 mm 2”. In: *IEEE International Solid-State Circuits Conference (ISSCC)*. 1999. DOI: 10.1109/ISSCC.1999.759268.

[49] Cheng-En Hsieh et al. “A Power- and Area-Efficient 4nm Self-Calibrated 12b/16GS/s Hierarchical Time-Interleaving ADC”. In: *IEEE International Solid-State Circuits Conference (ISSCC)*. 2025. DOI: 10.1109/ISSCC49661.2025.10904740.

[50] Sung-En Hsieh, Tzu-Chien Wu, and Chun-Chih Hou. “A 1.8-GHz 12-bit Pre-Sampling pipelined ADC with the reference buffer and OP power relaxations”. In: *IEEE International Solid-State Circuits Conference (ISSCC)*. 2023. DOI: 10.1109/ISSCC42615.2023.10067258.

[51] Cheng-Chung Hsu et al. “An 11-Bit 800-MS/s Time-Interleaved ADC with Digital Background Calibration”. In: *IEEE International Solid-State Circuits Conference (ISSCC)*. 2007. DOI: 10.1109/ISSCC.2007.373495.

[52] Y. Hu et al. “A 2.87μW 1kHz-BW 94.0dB-SNDR 2-0 MASH ADC using FIA with Dynamic-Body-Biasing Assisted CLS Technique”. In: *IEEE International Solid-State Circuits Conference (ISSCC)*. 2022. DOI: 10.1109/ISSCC42614.2022.9731544.

[53] Sheng-Jui Huang and Yung-Yu Lin. “A 1.2V 2MHz BW 0.084mm² CT $\Delta\Sigma$ ADC with -97.7dBc THD and 80dB DR Using Low-Latency DEM”. In: *IEEE International Solid-State Circuits Conference (ISSCC)*. 2009. DOI: 10.1109/ISSCC.2009.4977363.

[54] Y-C. Huang and T-C. Lee. “A 10b 100MS/s 4.5mW Pipelined ADC with a Time Sharing Technique”. In: *IEEE International Solid-State Circuits Conference (ISSCC)*. 2010. DOI: 10.1109/ISSCC.2010.5433927.

[55] D.J. Huber, R.J. Chandler, and A.A. Abidi. “A 10b 160MS/s 84mW 1V Subranging ADC in 90nm CMOS”. In: *IEEE International Solid-State Circuits Conference (ISSCC)*. 2007. DOI: 10.1109/ISSCC.2007.373490.

[56] Young-Deuk Jeon et al. “A 4.7mW 0.32mm² 10b 30MS/s Pipelined ADC Without a Front-End S/H in 90nm CMOS”. In: *IEEE International Solid-State Circuits Conference (ISSCC)*. 2007. DOI: 10.1109/ISSCC.2007.373491.

[57] Kyeongwon Jeong et al. “A 3.47 NEF 175.2dB FOMS Direct Digitization Front-End Featuring Delta Amplification for Enhanced Dynamic Range and Energy Efficiency in Bio-Signal Acquisition”. In: *IEEE International Solid-State Circuits Conference (ISSCC)*. 2025. DOI: 10.1109/ISSCC49661.2025.10904745.

[58] Joseph Ingino Jr. and Bruce Wooley. “A continuously-calibrated 10Msample/s 12b 3.3V ADC”. In: *IEEE International Solid-State Circuits Conference (ISSCC)*. 1998. DOI: 10.1109/ISSCC.1998.672409.

[59] T. Kang et al. “A Multimode 157μW 4-Channel 80dBA-SNDR Speech-Recognition Frontend With Self-DOA Correction Adaptive Beamformer”. In: *IEEE International Solid-State Circuits Conference (ISSCC)*. 2022. DOI: 10.1109/ISSCC42614.2022.9731571.

[60] Geunha Kim et al. “A 1V-Supply 1.85VPP-Input-Range 1kHz-BW 181.9dB-FOMDR 179.4dB-FOMSNDR 2nd-Order Noise-Shaping SARADC with Enhanced Input Impedance in 0.18μm CMOS”. In: *IEEE International Solid-State Circuits Conference (ISSCC)*. 2023. DOI: 10.1109/ISSCC42615.2023.10067844.

[61] Hwi-Cheol Kim, Deog-Kyoon Jeong, and Wonchan Kim. “A 30mW 8b 200MS/s pipelined CMOS ADC using a switched-opamp technique”. In: *IEEE International Solid-State Circuits Conference (ISSCC)*. 2005. DOI: 10.1109/ISSCC.2005.1493980.

[62] Jinseok Koh, Yunyoung Choi, and G. Gomez. “A 66dB DR 1.2V 1.2mW single-amplifier double-sampling 2nd-order $\Delta\Sigma$ ADC for WCDMA in 90nm CMOS”. In: *IEEE International Solid-State Circuits Conference (ISSCC)*. 2005. DOI: 10.1109/ISSCC.2005.1493923.

[63] Sandeep Santhosh Kumar et al. “A 750mW 24GS/s 12-bit Time Interleaved ADC for Direct RF Sampling in Modern Wireless Systems”. In: *IEEE International Solid-State Circuits Conference (ISSCC)*. 2023. DOI: 10.1109/ISSCC42615.2023.10067793.

[64] S.-U. Kwak, B.-S. Song, and K. Bacrania. “A 15 b 5 MSample/s low-spurious CMOS ADC”. In: *IEEE International Solid-State Circuits Conference (ISSCC)*. 1997. DOI: 10.1109/ISSCC.1997.585309.

[65] C. Y. Lee and U-K. Moon. “A 0.0375mm2 203.5μW 108.8dB DR DT Single-Loop DSM Audio ADC Using a Single- Ended Ring-Amplifier-Based Integrator in 180nm CMOS”. In: *IEEE International Solid-State Circuits Conference (ISSCC)*. 2022. DOI: 10.1109/ISSCC42614.2022.9731606.

[66] Jaewon Lee et al. “A 353mW 112Gb/s Discrete Multitone Wireline Receiver Datapath with Time-Based ADC in 5nm FinFET”. In: *IEEE International Solid-State Circuits Conference (ISSCC)*. 2025. DOI: 10.1109/ISSCC49661.2025.10904707.

[67] Jongmi Lee et al. “A 6th-Order Quadrature CTDSM using Double-OTA and Quadrature NSSAR with 171.3dB FoMs in 14nm”. In: *IEEE International Solid-State Circuits Conference (ISSCC)*. 2024. DOI: 10.1109/ISSCC49657.2024.10454568.

[68] Sangheon Lee et al. “A 1.2V High-Voltage-Tolerant Bootstrapped Analog Sampler in 12-bit SAR ADC Using 3nm GAA’s 0.7V Thin-Gate-Oxide Transistor”. In: *IEEE International Solid-State Circuits Conference (ISSCC)*. 2024. DOI: 10.1109/ISSCC49657.2024.10454351.

[69] Seung-Chul Lee et al. “A 10b 205MS/s 1.0mm² 90nm CMOS Pipeline ADC for Flat Panel Display Applications”. In: *IEEE International Solid-State Circuits Conference (ISSCC)*. 2007. DOI: 10.1109/ISSCC.2007.373492.

[70] Sewon Lee, Hyein Kang, and Minjae Lee. “A 2.72fJ/conv 13b 2MS/s SAR ADC Using Dynamic Capacitive Comparator with Wide Input Common Mode”. In: *IEEE International Solid-State Circuits Conference (ISSCC)*. 2024. DOI: 10.1109/ISSCC49657.2024.10454566.

[71] Manxin Li et al. “A Rail-to-Rail 12MS/s 91.3dB SNDR 94.1dB DR Two-Step SAR ADC with Integrated Input Buffer Using Predictive Level-Shifting”. In: *IEEE International Solid-State Circuits Conference (ISSCC)*. 2023. DOI: 10.1109/ISSCC42615.2023.10067703.

[72] Yong Lim et al. “A 2.08mW 64.4dB SNDR 400MS/s 12b Pipelined-SAR ADC using Mismatch and PVT Variation Tolerant Dynamically Biased Ring Amplifier in 8nm”. In: *IEEE International Solid-State Circuits Conference (ISSCC)*. 2024. DOI: 10.1109/ISSCC49657.2024.10454422.

[73] Chin-Yu Lin, Yen-Hsin Wei, and Tai-Cheng Lee. “A 10b 2.6GS/s Time-Interleaved SAR ADC with Background Timing-Skew Calibration”. In: *IEEE International Solid-State Circuits Conference (ISSCC)*. 2016. DOI: 10.1109/ISSCC.2016.7418110.

[74] Ying-Zu Lin et al. “A 40MHz-BW 320MS/s Passive Noise-Shaping SAR ADC with Passive Signal-Residue Summation in 14nm FinFET”. In: *IEEE International Solid-State Circuits Conference (ISSCC)*. 2019. DOI: 10.1109/ISSCC.2019.8662299.

[75] C-C. Liu et al. “A 10b 100MS/s 1.13mW SAR ADC with Binary-Scaled Error Compensation”. In: *IEEE International Solid-State Circuits Conference (ISSCC)*. 2010. DOI: 10.1109/ISSCC.2010.5433970.

[76] Chun-Cheng Liu. “A 0.35mW 12b 100MS/s SAR-Assisted Digital Slope ADC in 28nm CMOS”. In: *IEEE International Solid-State Circuits Conference (ISSCC)*. 2016. DOI: 10.1109/ISSCC.2016.7418107.

[77] J. Liu, M. Hassanpourghadi, and M. S-W. Chen. “A 10GS/s 8b 25fJ/c-s 2850um2 Two-Step Time-domain ADC Using Delay-Tracking Pipelined-SAR TDC with 500fs Time Step in 14nm CMOS Technology”. In: *IEEE International Solid-State Circuits Conference (ISSCC)*. 2022. DOI: 10.1109/ISSCC42614.2022.9731625.

[78] Q. Liu et al. “A 5GS/s 360MHz-BW 68dB-DR Continuous-Time 1-1-1 Filtering MASH ΔΣ ADC in 40nm CMOS”. In: *IEEE International Solid-State Circuits Conference (ISSCC)*. 2022. DOI: 10.1109/ISSCC42614.2022.9731789.

[79] W. Liu, P. Huang, and Y. Chiu. “A 12b 22.5/45MS/s 3.0mW 0.059mm² CMOS SAR ADC Achieving Over 90dB SFDR”. In: *IEEE International Solid-State Circuits Conference (ISSCC)*. 2010. DOI: 10.1109/ISSCC.2010.5433830.

[80] Zijian Liu et al. “A 10b 3GS/s Time-Domain ADC with Mutually Exclusive Metastability Correction and Wide Common-Mode Input”. In: *IEEE International Solid-State Circuits Conference (ISSCC)*. 2025. DOI: 10.1109/ISSCC49661.2025.10904818.

[81] Yaohui Luan et al. “A 12.2μW 99.6dB-SNDR 184.8dB-FOMS DT Zoom PPD ΔΣM with Gain-Embedded Bootstrapped Sampler”. In: *IEEE International Solid-State Circuits Conference (ISSCC)*. 2025. DOI: 10.1109/ISSCC49661.2025.10904732.

[82] Ewout Martens et al. “A 42GS/s 7b 16nm Massively Time-Interleaved Slope-ADC”. In: *IEEE International Solid-State Circuits Conference (ISSCC)*. 2024. DOI: 10.1109/ISSCC49657.2024.10454361.

[83] F. Michel and M. Steyaert. “A 250mv 7.5μw 61dB SndR cMoS Sc ΔΣ Modulator using a near-Threshold-voltage-Biased cMoS inverter Technique”. In: *IEEE International Solid-State Circuits Conference (ISSCC)*. 2011. DOI: 10.1109/ISSCC.2011.5746404.

[84] G. Mitteregger et al. “A 14b 20mW 640MHz CMOS CT ΔΣ ADC with 20MHz Signal Bandwidth and 12b ENOB”. In: *IEEE International Solid-State Circuits Conference (ISSCC)*. 2006. DOI: 10.1109/ISSCC.2006.1696042.

[85] A.K. Ong and B.A. Wooley. “A two-path bandpass ΣΔ modulator for digital IF extraction at 20 MHz”. In: *IEEE International Solid-State Circuits Conference (ISSCC)*. 1997. DOI: 10.1109/ISSCC.1997.585337.

[86] Sharvil Patil et al. “A 700MHz-BW –164dBFS/Hz-Small-Signal-NSD 703mW Continuous-Time Pipelined ADC with On-Chip Digital Reconstruction Achieving <-85dBFS HD3 using Digital Cancellation of DAC Errors”. In: *IEEE International Solid-State Circuits Conference (ISSCC)*. 2024. DOI: 10.1109/ISSCC49657.2024.10454477.

[87] Hendrik van der Ploeg and Robert Remmers. “A 3.3V 10b 25Msample/s two-step ADC in 0.35µm CMOS”. In: *IEEE International Solid-State Circuits Conference (ISSCC)*. 1999. DOI: 10.1109/ISSCC.1999.759267.

[88] C. Pochet and D. Hall. “A 4.4μW 2.5kHz-BW 92.1dB-SNDR 3rd-Order VCO-Based ADC with Pseudo Virtual Ground Feedforward Linearization”. In: *IEEE International Solid-State Circuits Conference (ISSCC)*. 2022. DOI: 10.1109/ISSCC42614.2022.9731549.

[89] Liang Qi et al. “A 76.6dB-SNDR 50MHz-BW 29.2mW Noise-Coupling-Assisted CT Sturdy MASH ΔΣ Modulator with 1.5b/4b Quantizers in 28nm CMOS”. In: *IEEE International Solid-State Circuits Conference (ISSCC)*. 2019. DOI: 10.1109/ISSCC.2019.8662529.

[90] Sourja Ray and Bang-Sup Song. “A 13b Linear 40MS/s Pipelined ADC with Self-Configured Capacitor Matching”. In: *IEEE International Solid-State Circuits Conference (ISSCC)*. 2006. DOI: 10.1109/ISSCC.2006.1696125.

[91] P. Schvan et al. “A 22GS/s 5b ADC in 130nm SiGe BiCMOS”. In: *IEEE International Solid-State Circuits Conference (ISSCC)*. 2006. DOI: 10.1109/ISSCC.2006.1696297.

[92] P. Schvan et al. “A 24GS/s 6b ADC in 90nm CMOS”. In: *IEEE International Solid-State Circuits Conference (ISSCC)*. 2008. DOI: 10.1109/ISSCC.2008.4523298.

[93] Y. Segal et al. “A 1.41pJ/b 224Gb/s PAM-4 SerDes Receiver with 31dB Loss Compensation”. In: *IEEE International Solid-State Circuits Conference (ISSCC)*. 2022. DOI: 10.1109/ISSCC42614.2022.9731794.

[94] D. Senderowicz et al. “Low-voltage double-sampled ΣΔ converters”. In: *IEEE International Solid-State Circuits Conference (ISSCC)*. 1997. DOI: 10.1109/ISSCC.1997.585336.

[95] Junhua Shen et al. “A 12GS/s 9b 16× Time-Interleaved SAR ADC in 16nm FinFET”. In: *IEEE International Solid-State Circuits Conference (ISSCC)*. 2025. DOI: 10.1109/ISSCC49661.2025.10904660.

[96] Y. Shimizu et al. “A Split-Load Interpolation-Amplifier-Array 300MS/s 8b Subranging Adc in 90nm CMOS”. In: *IEEE International Solid-State Circuits Conference (ISSCC)*. 2008. DOI: 10.1109/ISSCC.2008.4523302.

[97] Yasuhide Shimizu et al. “A 30mW 12b 40MS/s Subranging ADC with a High-Gain Offset-Canceling Positive-Feedback Amplifier in 90nm Digital CMOS”. In: *IEEE International Solid-State Circuits Conference (ISSCC)*. 2006. DOI: 10.1109/ISSCC.2006.1696120.

[98] P.G.R. Silva et al. “An 118dB DR CT IF-to-Baseband ΣΔ Modulator for AM/FM/IBOC Radio Receivers”. In: *IEEE International Solid-State Circuits Conference (ISSCC)*. 2006. DOI: 10.1109/ISSCC.2006.1696044.

[99] Anand Subramanian et al. “A 118.5dBA DR 3.3mW Audio ADC with a Class-B Resistor DAC, Non-Overlap DEM and Continuous-Time Quantizer”. In: *IEEE International Solid-State Circuits Conference (ISSCC)*. 2024. DOI: 10.1109/ISSCC49657.2024.10454526.

[100] A. Tabatabaei et al. “A dual channel ΣΔ ADC with 40MHz aggregate signal bandwidth”. In: *IEEE International Solid-State Circuits Conference (ISSCC)*. 2003. DOI: 10.1109/ISSCC.2003.1234210.

[101] Yuko Tamba and Kazuo Yamakido. “A CMOS 6b 500MSample/s ADC for a hard disk drive read channel”. In: *IEEE International Solid-State Circuits Conference (ISSCC)*. 1999. DOI: 10.1109/ISSCC.1999.759272.

[102] Yunsong Tao et al. “A 4.8GS/s 7-ENoB Time-Interleaved SAR ADC with Dither-Based Background Timing-Skew Calibration and Bit-Distribution-Based Background Ping-Pong Comparator Offset Calibration”. In: *IEEE International Solid-State Circuits Conference (ISSCC)*. 2024. DOI: 10.1109/ISSCC49657.2024.10454299.

[103] Yunsong Tao et al. “An 8b 10GS/s 2-Channel Time-Interleaved Pipelined ADC with Concurrent Residue Transfer and Quantization, and Automatic Buffer Power Gating”. In: *IEEE International Solid-State Circuits Conference (ISSCC)*. 2025. DOI: 10.1109/ISSCC49661.2025.10904751.

[104] Bram Veraverbeke and Filip Tavernier. “A Cryo-CMOS 800MS/s 7b CI-SAR with only 4fF Input Capacitance and 64dB SFDR”. In: *IEEE International Solid-State Circuits Conference (ISSCC)*. 2025. DOI: 10.1109/ISSCC49661.2025.10904533.

[105] Naveen Verma and Anantha Chandrakasan. “A 25μW 100kS/s 12b ADC for Wireless Micro-Sensor Applications”. In: *IEEE International Solid-State Circuits Conference (ISSCC)*. 2006. DOI: 10.1109/ISSCC.2006.1696122.

[106] K. Vleugels, S. Rabii, and B.A. Wooley. “A 2.5 V broadband multi-bit ΣΔ modulator with 95 dB dynamic range”. In: *IEEE International Solid-State Circuits Conference (ISSCC)*. 2001. DOI: 10.1109/ISSCC.2001.912541.

[107] Patrick Vogelmann, Michael Haas, and Maurits Ortmanns. “A 1.1mW 200kS/s Incremental ΔΣ ADC with a DR of 91.5dB Using Integrator Slicing for Dynamic Power Reduction”. In: *IEEE International Solid-State Circuits Conference (ISSCC)*. 2018. DOI: 10.1109/ISSCC.2018.8310271.

[108] M. Waltari et al. “A self-calibrated pipeline ADC with 200MHz IF-sampling frontend”. In: *IEEE International Solid-State Circuits Conference (ISSCC)*. 2002. DOI: 10.1109/ISSCC.2002.993058.

[109] Chi-Yun (Stanley) Wang et al. “An 80MHz-BW 31.9fJ/conv-step Filtering ΔΣ ADC with a Built-In DAC-Segmentation/ELDCompensation 6b 960MS/s SAR-Quantizer in 28nm LP for 802.11ax Applications”. In: *IEEE International Solid-State Circuits Conference (ISSCC)*. 2019. DOI: 10.1109/ISSCC.2019.8662416.

[110] Yi-Hu Wang and Soon-Jyh Chang. “A 7b 4.5GS/s 4× Interleaved SAR ADC with Fully On-Chip Background Timing Skew Calibration”. In: *IEEE International Solid-State Circuits Conference (ISSCC)*. 2023. DOI: 10.1109/ISSCC42615.2023.10067573.

[111] J-C. Wang and T-H. Kuo. “A 0.82mW 14b 130MS/s Pipelined-SAR ADC with a Distributed Averaging Correlated Level Shifting (DACLS) Ringamp and Bypass-Window Backend”. In: *IEEE International Solid-State Circuits Conference (ISSCC)*. 2022. DOI: 10.1109/ISSCC42614.2022.9731546.

[112] Jia-Ching Wang and Tai-Haur Kuo. "A 3-mW 2.7-GS/s 8b Subranging ADC with Multiple-Reference-Embedded Comparators". In: *IEEE International Solid-State Circuits Conference (ISSCC)*. 2023. DOI: 10.1109/ISSCC42615.2023.10067498.

[113] R. Wang et al. "A 3.3 mW 12 MS/s 10b pipelined ADC in 90 nm digital CMOS". In: *IEEE International Solid-State Circuits Conference (ISSCC)*. 2005. DOI: 10.1109/ISSCC.2005.1493977.

[114] T. Wang et al. "An 84dB-SNDR Low-OSR 4th-Order Noise-Shaping SAR with an FIA-Assisted EF-CRFF Structure and Noise-Mitigated Push-Pull Buffer-in-Loop Technique". In: *IEEE International Solid-State Circuits Conference (ISSCC)*. 2022. DOI: 10.1109/ISSCC42614.2022.9731771.

[115] H. Wei et al. "A 0.024mm² 8b 400MS/s SaR adc with 2b/cycle and Resistive dac in 65nm cMoS". In: *IEEE International Solid-State Circuits Conference (ISSCC)*. 2011. DOI: 10.1109/ISSCC.2011.5746276.

[116] Amy Whitcombe et al. "A 76mW 40GS/s 7b Time-Interleaved Hybrid Voltage/Time-Domain ADC with Common-Mode Input Tracking". In: *IEEE International Solid-State Circuits Conference (ISSCC)*. 2024. DOI: 10.1109/ISSCC49657.2024.10454355.

[117] Jianxiong Xu et al. "Event-Based Spatially Zooming Neural Interface IC with 10nW/Input Reconfigurable-Inverter Fabric and Input-Adaptive Quantization". In: *IEEE International Solid-State Circuits Conference (ISSCC)*. 2025. DOI: 10.1109/ISSCC49661.2025.10904733.

[118] S. Yan and E. Sanchez-Sinencio. "A continuous-time ΣΔ modulator with 88dB dynamic range and 1.1MHz signal bandwidth". In: *IEEE International Solid-State Circuits Conference (ISSCC)*. 2003. DOI: 10.1109/ISSCC.2003.1234208.

[119] L. Yao, M. Steyaert, and W. Sansen. "A 1 V 88 dB 20 kHz ΣΔ modulator in 90 nm CMOS". In: *IEEE International Solid-State Circuits Conference (ISSCC)*. 2004. DOI: 10.1109/ISSCC.2004.1332603.

[120] F. M. Yaul and A. P. Chandrakasan. "A 10b 0.6nW leakage SAR ADC with data-dependent energy savings using LSB-first successive approximation". In: *IEEE International Solid-State Circuits Conference (ISSCC)*. 2014. DOI: 10.1109/ISSCC.2014.6757398.

[121] Siyuan Ye et al. "A 2mW 70.7dB SNDR 200MS/s Pipelined-SAR ADC with Continuous-Time SAR-Assisted Detect-and-Skip and Open-then-Close Correlated Level Shifting". In: *IEEE International Solid-State Circuits Conference (ISSCC)*. 2024. DOI: 10.1109/ISSCC49657.2024.10454412.

[122] Siyuan Ye et al. "A Rail-to-Rail 3rd-Order Noise-Shaping SAR ADC Achieving 105.4dB SFDR with Integrated Input Buffer Using Continuous-Time Correlated Level Shifting". In: *IEEE International Solid-State Circuits Conference (ISSCC)*. 2025. DOI: 10.1109/ISSCC49661.2025.10904773.

[123] Serdar Abdullah Yonar et al. “An 8b 1.0-to-1.25GS/s 0.7-to-0.8V Single-Stage Time-Based Gated-Ring-Oscillator ADC with 2X- Interpolating Sense-Amplifier-Latches”. In: *IEEE International Solid-State Circuits Conference (ISSCC)*. 2023. DOI: 10.1109/ISSCC42615.2023.10067745.

[124] Kentaro Yoshioka et al. “A 0.7V 12b 160MS/s 12.8fJ/conv-step Pipelined-SAR ADC in 28nm CMOS with Digital Amplifier Technique”. In: *IEEE International Solid-State Circuits Conference (ISSCC)*. 2017. DOI: 10.1109/ISSCC.2017.7870469.

[125] M. Yoshioka et al. “A 0.8V 10b 80MS/s 6.5mW Pipelined ADC with Regulated Overdrive Voltage Biasing”. In: *IEEE International Solid-State Circuits Conference (ISSCC)*. 2007. DOI: 10.1109/ISSCC.2007.373489.

[126] M. Yoshioka et al. “A 10 b 125 MS/s 40 mW pipelined ADC in 0.18 μm CMOS”. In: *IEEE International Solid-State Circuits Conference (ISSCC)*. 2005. DOI: 10.1109/ISSCC.2005.1493979.

[127] M. Yoshioka et al. “A 10b 50MS/s 820μW SAR ADC with On-Chip Digital Calibration”. In: *IEEE International Solid-State Circuits Conference (ISSCC)*. 2010. DOI: 10.1109/ISSCC.2010.5433965.

[128] Jiang Yu and F. Maloberti. “A low-power multi-bit $\Delta\Sigma$ modulator in 90nm digital CMOS without DEM”. In: *IEEE International Solid-State Circuits Conference (ISSCC)*. 2005. DOI: 10.1109/ISSCC.2005.1493922.

[129] M. Zhan et al. “A 0.004mm2 200MS/s Pipelined SAR ADC with kT/C Noise Cancellation and Robust Ring-Amp”. In: *IEEE International Solid-State Circuits Conference (ISSCC)*. 2022. DOI: 10.1109/ISSCC42614.2022.9731599.

[130] Mingtao Zhan, Lu Jie, and Nan Sun. “A 10mW 10-ENoB 1GS/s Ring-Amp-Based Pipelined TI-SAR ADC with Split MDAC and Switched Reference Decoupling Capacitor”. In: *IEEE International Solid-State Circuits Conference (ISSCC)*. 2023. DOI: 10.1109/ISSCC42615.2023.10067475.

[131] Hongshuai Zhang et al. “A 25MHz-BW 77.2dB-SNDR 2nd-Order Gain Error Shaping and NS Pipelined SAR ADC Based on Quantization-Prediction-Unrolled Scheme”. In: *IEEE International Solid-State Circuits Conference (ISSCC)*. 2023. DOI: 10.1109/ISSCC42615.2023.10067438.

[132] Minglei Zhang et al. “A 0.6V 13b 20MS/s Two-Step TDC-Assisted SAR ADC with PVT Tracking and Speed-Enhanced Techniques”. In: *IEEE International Solid-State Circuits Conference (ISSCC)*. 2019. DOI: 10.1109/ISSCC.2019.8662350.

[133] Yanbo Zhang et al. “A Single-channel 70dB-SNDR 100MHz-BW 4th-Order Noise-Shaping Pipeline SAR ADC with Residue Amplifier Error Shaping”. In: *IEEE International Solid-State Circuits Conference (ISSCC)*. 2023. DOI: 10.1109/ISSCC42615.2023.10067687.

[134] Yannan Zhang et al. “A 72GS/s 9b Time-Interleaved Pipeline-SAR ADC Achieving 55.3/49.3dB SFDR at 20GHz/Nyquist Inputs in 16nm FinFET”. In: *IEEE International Solid-State Circuits Conference (ISSCC)*. 2025. DOI: 10.1109/ISSCC49661.2025.10904672.

[135] H. Zhao and F. F. Dai. “A 0.97mW 260MS/s 12b Pipelined-SAR ADC with Ring-TDC-Based Fine Quantizer for PVT Robust Automatic Cross-Domain Scale Alignment”. In: *IEEE International Solid-State Circuits Conference (ISSCC)*. 2022. DOI: 10.1109/ISSCC42614.2022.9731702.

[136] Han Zhao et al. “A Fully Dynamic Noise-Shaping SAR ADC Achieving 120dB SNDR and 189dB FoMS in 1kHz BW”. In: *IEEE International Solid-State Circuits Conference (ISSCC)*. 2025. DOI: 10.1109/ISSCC49661.2025.10904778.

[137] Hongzhi Zhao et al. “A 2×-Interleaved 9b 2.8GS/s 5b/cycle SAR ADC with Linearized Configurable V2T Buffer Achieving >50dB SNDR at 3GHz Input”. In: *IEEE International Solid-State Circuits Conference (ISSCC)*. 2023. DOI: 10.1109/ISSCC42615.2023.10067627.

[138] Junlin Zhong et al. “A PVT-Robust 2× Interleaved 2.2GS/s ADC with Gated-CCRO-Based Quantizer Shared Across Channels and Steps Achieving >4.5GHz ERBW”. In: *IEEE International Solid-State Circuits Conference (ISSCC)*. 2025. DOI: 10.1109/ISSCC49661.2025.10904585.